Supporting Information

NIR-II Photothermal Conversion and Imaging Based on a Cocrystal containing Twisted Components

Tao Li,[a,b] Jia-Chuan Liu,[a] En-Ping Liu,[c] Bai-Tong Liu,[d] Jing-Yu Wang,[a] Pei-Yu Liao,[a] Jian-Hua Jia,[a] Yuanning Feng,[*,b] and Ming-Liang Tong[*,a]

a Key Laboratory of Bioinorganic and Synthetic Chemistry of Ministry of Education, School of Chemistry, Institute of Green Chemistry and Molecular Engineering, Sun Yat-Sen University, Guangzhou, Guangdong 510006, China

b Department of Chemistry and Biochemistry, University of Oklahoma, 101 Stephenson Parkway, Norman, Oklahoma 73019, United States

c School of Materials Science and Engineering, Tianjin University, Tianjin 300072, China

d Department of Chemistry, Northwestern University, 2145 Sheridan Road, Evanston, Illinois 60208, United States

*E-mail: tongml@mail.sysu.edu.cn; yf@ou.edu

Table of Content

1. General Information

Unless otherwise mentioned, all reagents and solvents were purchased from commercial sources and used as received without further purification.

The C, H, and N elemental analyses were carried out using an Elementar Vario-EL CHNS elemental analyzer. Thermogravimetric analysis was carried out on a TG-209/Vector-2 thermogravimetric analyzer 2, and the dried crystalline samples were heated at a rate of 5 up to 800 °C per minute and then cooled to room temperature under N_2 atmosphere. Powder X-ray diffraction (PXRD) patterns were performed on a Rigaku Smartlab X-Ray diffractometer with Cu-Kα (λ = 1.54178 Å) radiation. UV–Vis–NIR diffuse reflectance spectra (DRS) were recorded using a UV–Vis spectrophotometer (Shimadzu UV-3600Plus) equipped with an integrating sphere, and $BaSO_4$ powder was used as the reference for the baseline correction. Electron paramagnetic resonance (EPR) data were collected in the X-band at room temperature on a Bruker A300 spectrometer. The solid-state fluorescent spectra were measured on an Edinburgh FLS-980 Fluorescence spectrometer equipped with a visible photomultiplier tube (PMT) and a NIR PMT upon excitation with a continuous Xenon lamp. X-Ray photoelectron spectroscopy (XPS) measurements were performed on a Thermo Fisher Scientific ESCALAB Xi+ system with an Al Kα source. Sequential XPS spectra were recorded by scanninthete electron analyzer from 100 to 75 eV in 0.05 eV increments under 20.0 eV pass energy. Time-resolved optical spectroscopy: the femtosecond transient absorption (fs-TA) spectra were recorded on a Helios Fire spectrometer (Ultrafast System). The excitation pulse (400 nm, 25 μW) is a regeneratively amplified Ti: Sapphire laser source (Coherent Legend, 800 nm, 150 fs, 5 mJ per pulse, and 1 kHz repetition rate). Fs-TA data were background- and chirp-corrected using Surface Xplorer 4.5 (Ultrafast Systems, LLC) and then analyzed in MATLAB using previously reported methods. The data at selected wavelengths were globally fit to the solution of a sequential three-site model convoluted with a 0.3 ps Gaussian instrument response function. The resulting time-dependent populations were then used to derive the evolution-associated spectra.

2.Experimental Section

Cocrystal Preparation. 1,6,7,8-Tetrachloro-3,4,9,10-perylenetetracarboxylic dianhydride (TCPDA, 40 mg) was dissolved in 20 mL THF using ultrasonication and heat. Above supernatant (1 mL) was added to a 20-mL vial containing 10 mg of tetrathiafulvalene (TTF). The mixture was treated by ultrasonication for 5 min, given rise to a pellucid dark red solution. After loosening silicone-lined cap and evaporating THF slowly at room temperature for one day, dark needle-like single crystals was appeared (**Figure S1**) as the TTF–TCPDA cocrystal (6.1 mg, 61% yield), which was chosen for single-crystal X-ray diffraction analysis.

Photothermal Measurement. The TTF–TCPDA crystalline powder (30 mg) was spread on a quartz slide at a distance of 0.7 cm from the 1064 nm laser (Beijing Sitong Boyuan Laser Technology Co., Ltd, Beijing, China). The laser intensity was adjusted from 0.1 to 0.5 $W \cdot cm^{-2}$. The temperature changes during the light irradiation were recorded by an infrared camera (Ti450, Fluke) and infrared photos recording real-time temperatures were extracted from the video by data statistics.

Electrochemistry Measurement. A CH instruments electrochemistry workstation (CHI660A) was used for electrochemistry experiments. We used a platinum wire as the counter electrode, glassy carbon as the working electrode, and 0.1 mol/L silver ion MeCN standard solution as the reference electrode for three electrode pulse voltammetry experiments. TTF, TCPDA, and TTF–TCPDA were dissolved in 15 mL of THF and 5 mL of MeCN to obtain 0.01 mmol solutions, respective. The scan rates were set at 30, 50 and 70 mV/s, respectively.

3. (Super)structural Determination

Single-crystal X-ray diffraction data of TTF–TCPDA were collected at room temperature on a Hybrid Pixel Array detector equipped with Ga-Kα radiation (λ = 1.3405 Å). Crystallographic data of crystal TCPDA was collected on Bruker D8 diffractometer with graphite-monochromatic Cu-Kα radiation (λ = 1.54184 Å) at room temperature. (Super)structures were solved by direct method and refined using Olex 2 integrated with the SHELXL-2016 software package.

Table.S1 Crystal data and (super)structures refinement results

Compound	TTF–TCPDA	TCPDA
CCDC Number	2219621	2219622
Empirical formula	$C_{40}H_{20}Cl_4O_7S_8$	$C_{24}H_4Cl_4O_6$
Formula weight	1010.84	530.07
Temperature/K	298	293
Crystal system	orthorhombic	monoclinic
Space group	$P2_12_12$	$P2_1/n$
a/Å	17.9065(3)	13.15240(16)
b/Å	15.4002(3)	10.75525(12)
c/Å	7.39430(10)	14.18556(17)
α/°	90	90
β/°	90	111.4740(14)
γ/°	90	90
V/Å^3	2039.08(6)	1867.36(4)
Z	2	4
ρ_{calc}/g cm^{-3}	1.646	1.885
μ/mm^{-1}	4.531	6.2
F(000)	1024.0	1056
Radiation	GaKα (λ = 1.3405)	CuKα (λ = 1.54184)
2Θrange for data collection/°	6.582 to 121.836	7.85 to 143.03
Index range	$-23 \le h \le 22$ $-20 \le k \le 20$ $-9 \le l \le 9$	$-16 \le h \le 15$ $-8 \le k \le 13$ $-11 \le l \le 17$
Reflections collected	59114	7003
Independent reflection	4692 [R_{int} = 0.0695, R_{sigma} = 0.0204]	3560 [R_{int} = 0.0241, R_{sigma} = 0.0324]
Data/restraint/parameter	4692/0/267	3560/0/317
Goodness-of-fit on F^2	1.070	1.048
Final R indexe [I>=2σ (I)]	R_1 = 0.0555, wR_2 = 0.1774	R_1 = 0.0327, wR_2 = 0.0873
Final R indexe [all data]	R_1 = 0.0592, wR_2 = 0.1827	R_1 = 0.0350, wR_2 = 0.0896
Largest diff. peak/hole / e Å^{-3}	0.54/–0.54	0.79/–0.42

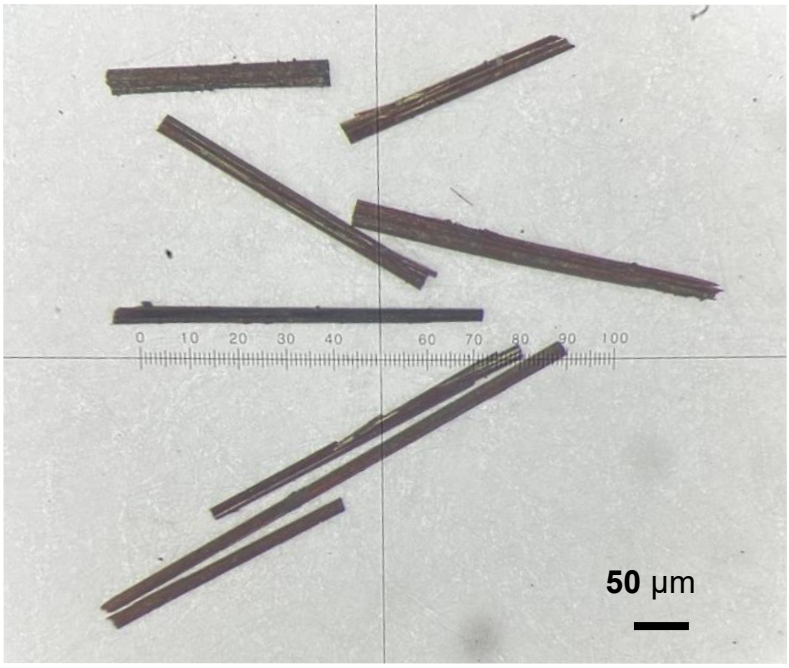

Figure S1. Optical micrograph of TTF–TCPDA showing its needle-like cocrystals

C1-C4	1.34
S1-C1	1.75
S2-C1	1.75
S1-C3	1.73
S2-C2	1.73
C2-C3	1.30
S3-C4	1.75
S4-C4	1.75
S3-C6	1.73
S4-C5	1.73
C5-C6	1.30

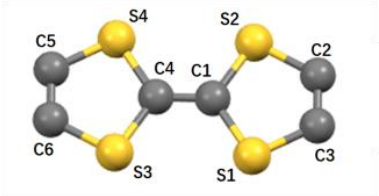

Scheme S1. Selected structural parameters for TTF[1] alone

C1-C4	1.32
S1-C1	1.75
S2-C1	1.76
S1-C3	1.74
S2-C2	1.71
C2-C3	1.27
S3-C4	1.74
S4-C4	1.76
S3-C6	1.81
S4-C5	1.51
C5-C6	1.36

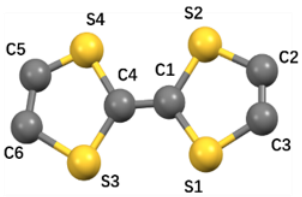

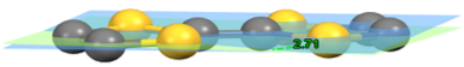

Scheme S2. Selected structural parameters for TTF component in TTF–TCPDA cocrystals

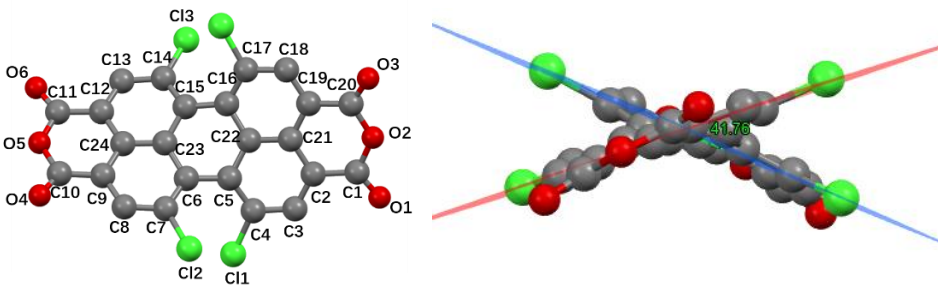

C1-C2	1.481	C12-C13	1.377	C6-C23	1.433	O2-C20	1.382
C2-C3	1.366	C13-C14	1.404	C9-C24	1.411	O3-C20	1.185
C3-C4	1.408	C14-C15	1.398	C12-C24	1.413	O4-C10	1.197
C4-C5	1.395	C15-C16	1.472	C15-C23	1.429	O5-C10	1.391
C5-C6	1.471	C16-C17	1.399	C16-C22	1.429	O5-C11	1.393
C6-C7	1.393	C17-C18	1.407	C19-C21	1.407	O6-C11	1.193
C7-C8	1.406	C18-C19	1.378	C21-C22	1.412	Cl1-C4	1.723
C8-C9	1.379	C19-C20	1.482	C23-C24	1.409	Cl2-C7	1.724
C9-C10	1.468	C2-C21	1.414	O1-C1	1.191	Cl3-C14	1.724
C11-C12	1.473	C5-C22	1.431	O2-C1	1.390	Cl4-C17	1.725

Scheme S3. Selected structural parameters for TCPDA alone

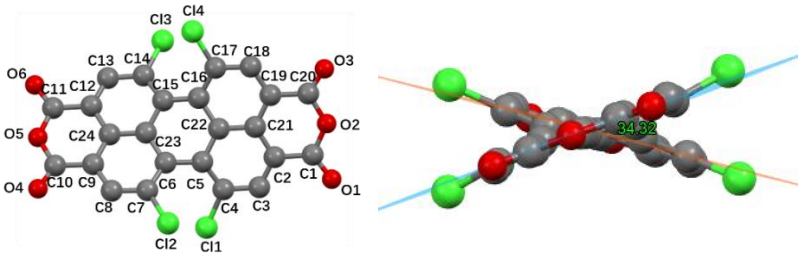

C1-C2	1.492	C12-C13	1.356	C6-C23	1.426	O2-C20	1.384
C2-C3	1.356	C13-C14	1.398	C9-C24	1.404	O3-C20	1.174
C3-C4	1.398	C14-C15	1.394	C12-C24	1.407	O4-C10	1.174
C4-C5	1.394	C15-C16	1.451	C15-C23	1.437	O5-C10	1.384
C5-C6	1.451	C16-C17	1.414	C16-C22	1.426	O5-C11	1.361
C6-C7	1.414	C17-C18	1.387	C19-C21	1.404	O6-C11	1.205
C7-C8	1.387	C18-C19	1.365	C21-C22	1.414	Cl1-C4	1.733
C8-C9	1.365	C19-C20	1.477	C23-C24	1.414	Cl2-C7	1.725
C9-C10	1.477	C2-C21	1.407	O1-C1	1.208	Cl3-C14	1.733
C11-C12	1.492	C5-C22	1.437	O2-C1	1.361	Cl4-C17	1.725

Scheme S4. Selected structural parameters for TCPDA component in TTF–TCPDA cocrystals

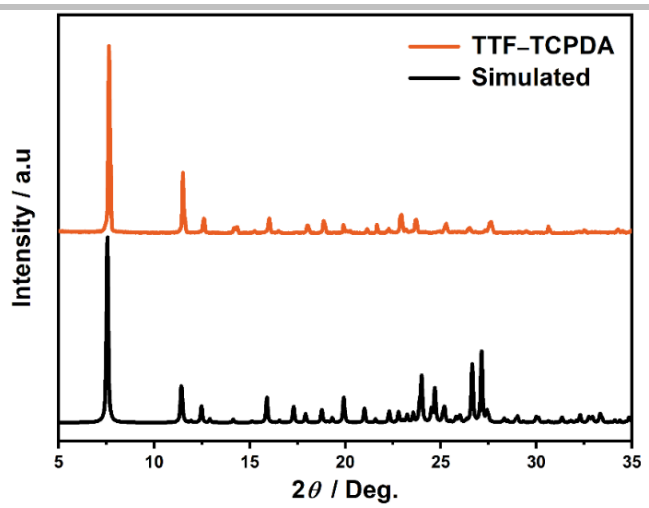

Figure S2. PXRD Patterns of the synthetic (orange) and simulated (black) TTF–TCPDA cocrystals

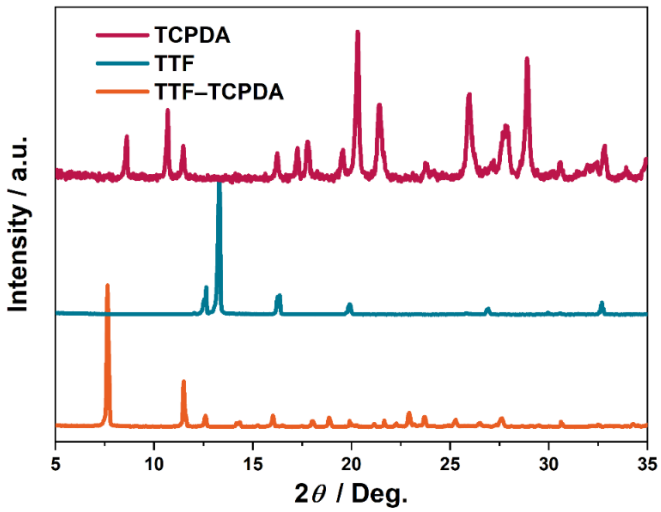

Figure S3. PXRD Patterns of synthetic TTF (blue), TCPDA (red) and TTF–TCPDA (orange) (co)crystals

4. Physical Characterization

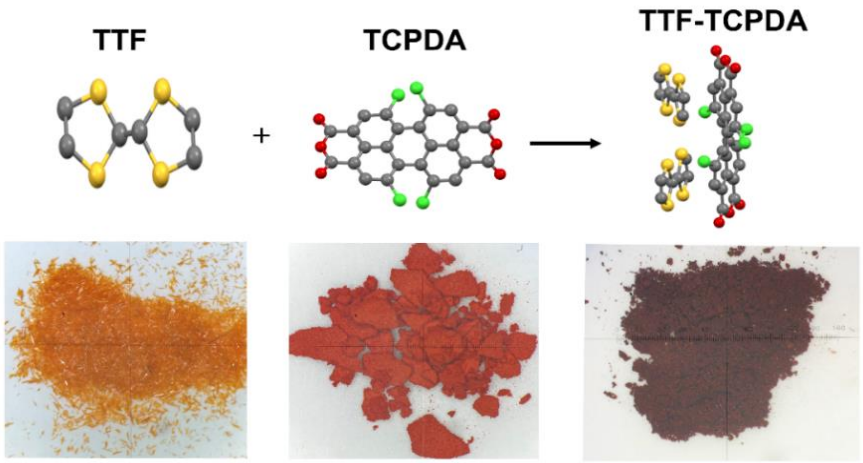

Figure S4. Stick-and-ball representations of the (super)structures of TTF, TCPDA and TTF–TCPDA (top) and photographs of their powders (bottom)

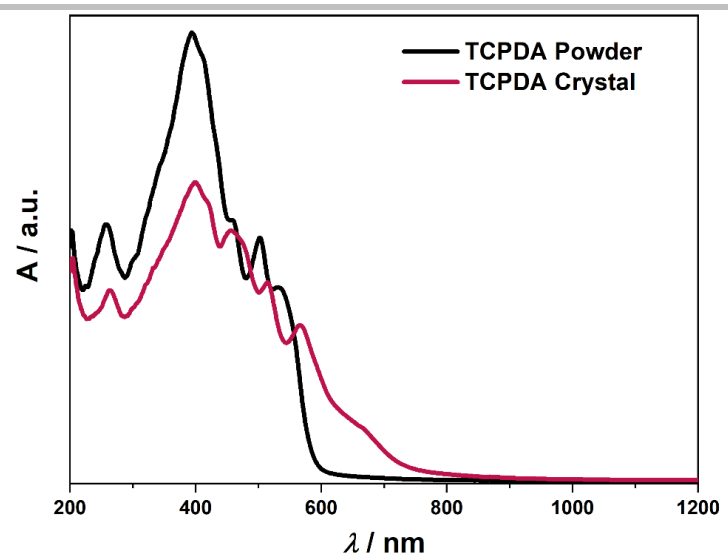

Figure S5. Overlaid UV–Vis–NIR diffuse reflectance spectra of TCPDA powder (black) and crystal (red)

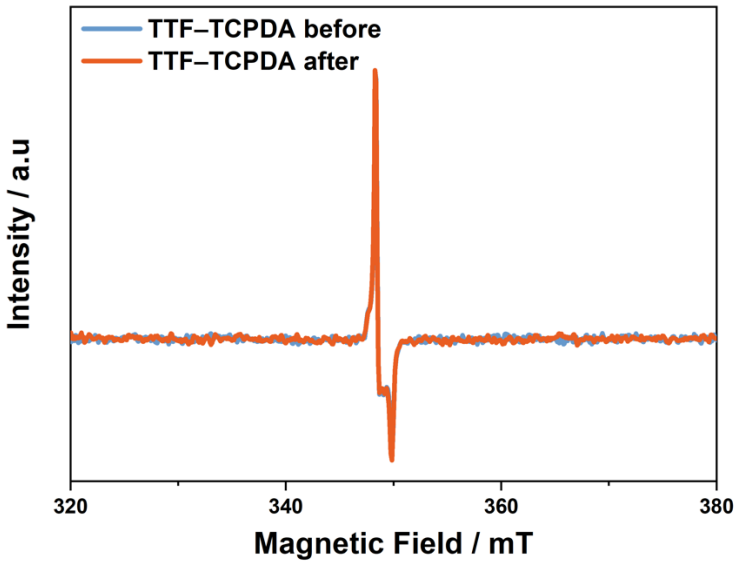

Figure S6. Overlaid EPR spectra of TTF–TCPDA radical before (blue) and after (orange) the light irradiation for 10 min at room temperature

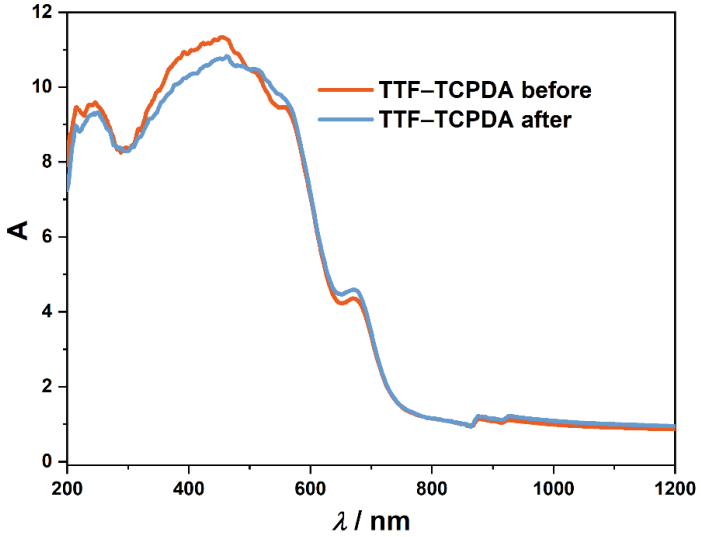

Figure S7. Overlaid UV–Vis–NIR diffuse reflectance spectra of TTF–TCPDA before (orange) and after (blue) the light irradiation for 10 min at room temperature

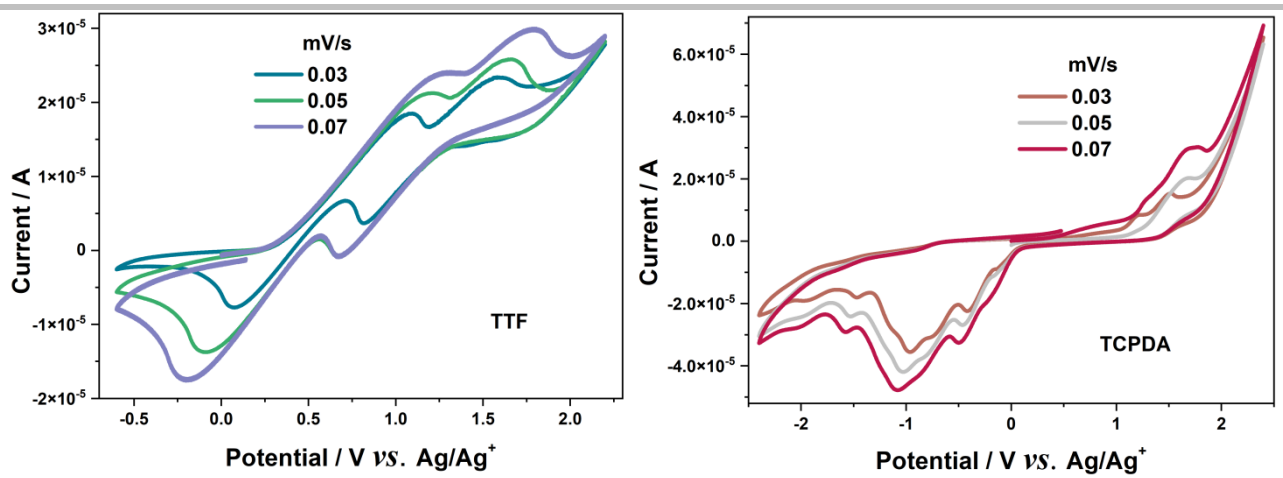

Figure S8. Overlaid cyclic voltammetry graphs of TTF (left) and TCPDA (right) at scan rates of 0.03, 0.05 and 0.07 mV/s, respectively

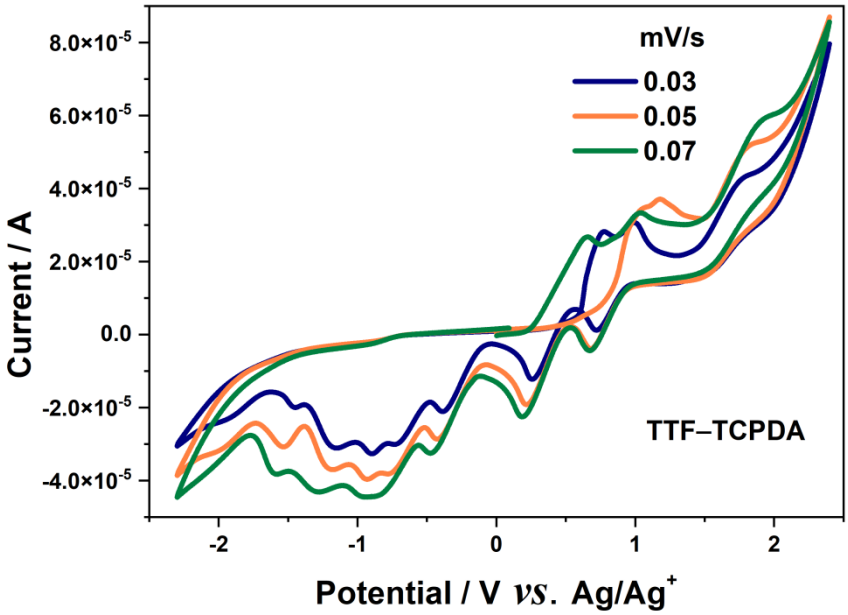

Figure S9. Overlaid cyclic voltammetry graph of TTF–TCPDA at scan rates of 0.03, 0.05 and 0.07 mV/s, respectively

5. Theoretical Calculation

The B3LYP functional[2] and 6-311+G** basis set were employed in this article to perform orbital and spin characteristic calculations, while UB3LYP functional was used in time-dependent density functional theory (TD-DFT) calculations. DFT-D3 (BJ) correction[3] was taken into account. (Super)structures used in all the calculation except IRC mission were derived from single-crystal X-ray diffraction data. When calculating the interaction energy (ΔE_{int}) between TTF and TCPDA components, the basis set superposition error[4] (BSSE) was included in the calculation. The B3LYP functional and def2-SVP basis set were used in optimization and intrinsic reaction coordinate mission. The Gaussian 09 package[5] was used for all of the calculation. Multiwfn software[6] was used to analyze wavefunction data produced by Gaussian. Visual molecular dynamics software[7] was used to visualize calculation results.

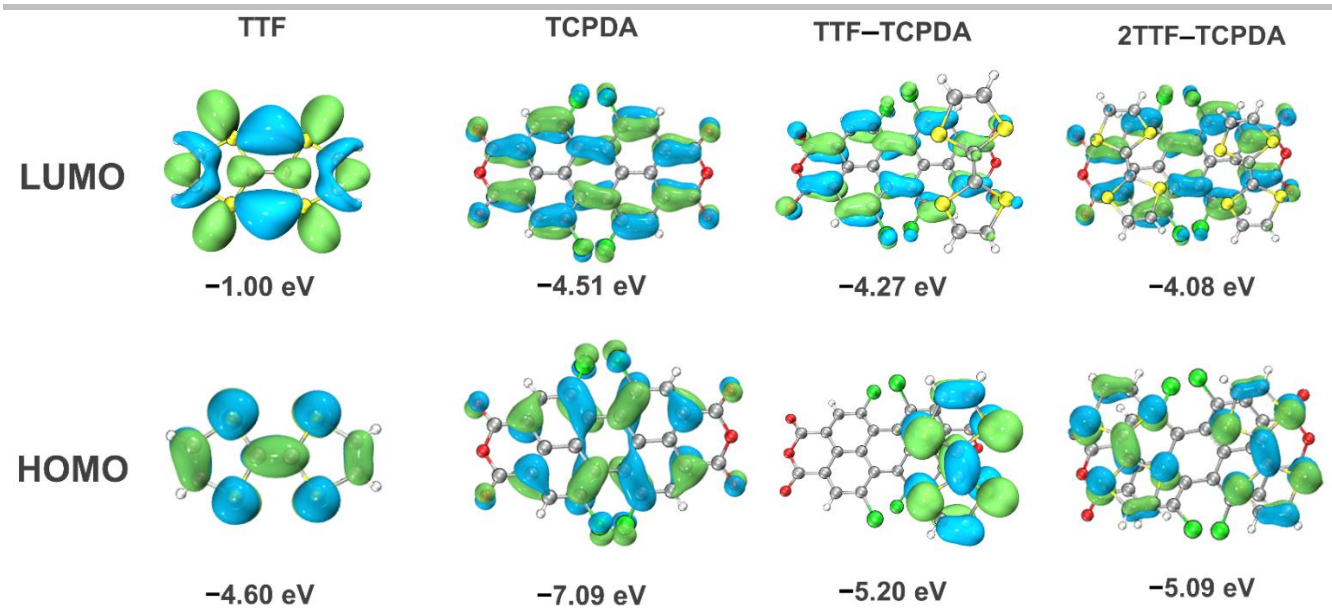

Figure S10. Frontier molecular orbitals of TTF, TCPDA, TTF–TCPDA and 2TTF–TCPDA in the TTF–TCPDA cocrystal, respectively

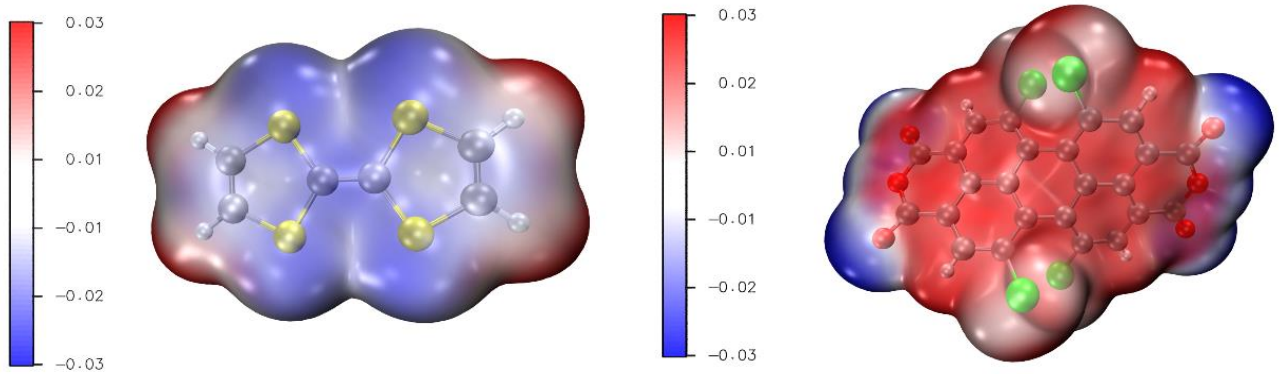

Figure S11. Electrostatic potential (ESP) analyses of TTF (left) and TCPDA (right)

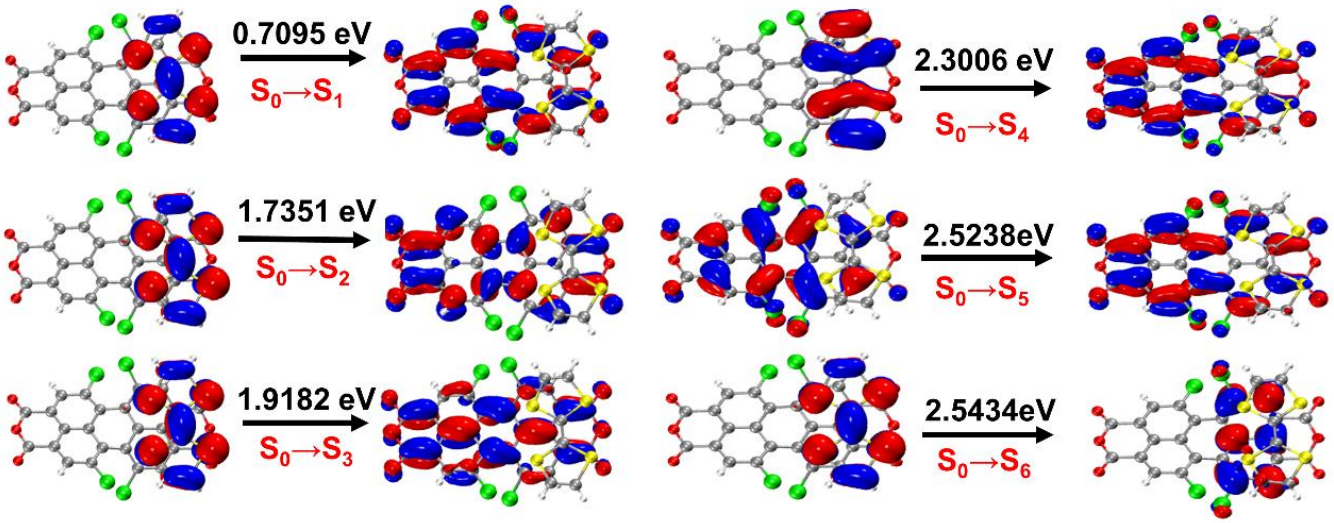

Figure S12. Natural transition orbitals[8] of S_0 to singlet excited states on a D–A dimer from infinite D–A stacking

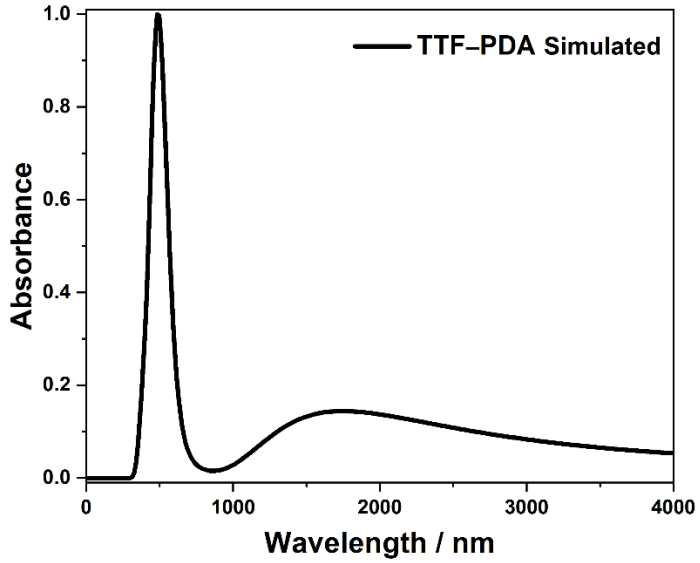

Figure S13. Calculated absorption spectra of TTF–TCPDA using TD-DFT method

Table S2. TD-DFT Calculations at UB3LYP/6-311+G** D3 (BJ)level for the transition from S_0 to the first six excited states of the D–A dimer in TTF–TCPDA

Excited state	Calculated λ / nm	Oscillator strength	Energy of transition / eV
S_1	1747.5	0.0894	0.7095
S_2	714.58	0.0072	1.7351
S_3	646.34	0.0068	1.9182
S_4	538.92	0.0214	2.3006
S_5	491.25	0.4210	2.5238
S_6	487.48	0.1701	2.5434

6. NIR-II Photothermal Conversion Measurement

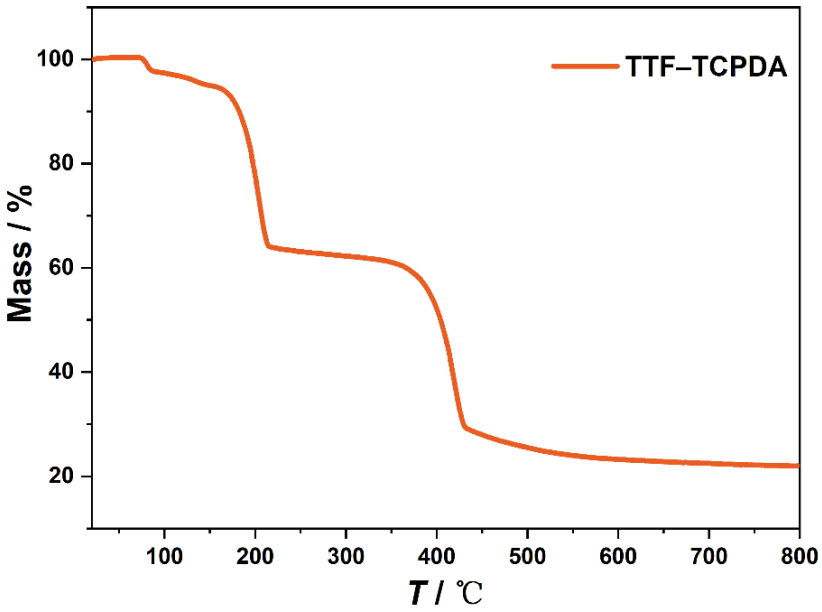

Figure S14. TGA Curves of as-synthesized TTF–TCPDA showing it is thermally stable lower than 175 °C

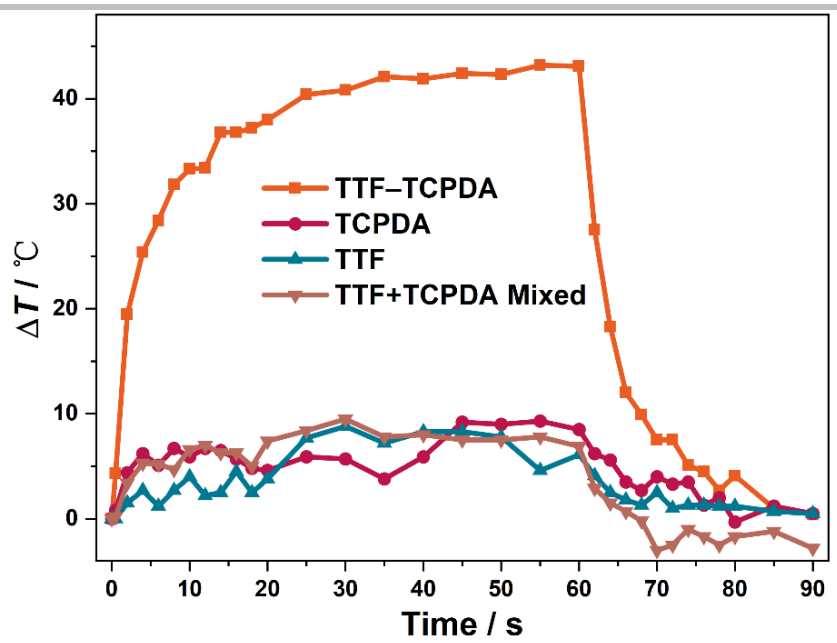

Figure S15. Overlaid photothermal conversion curves of TTF (orange), TCPDA (blue), TTF+TCPDA mixture (cyan), and TTF–TCPDA cocrystal (brown) under a 1064 nm laser (0.1 W·cm^{-2}) irradiation

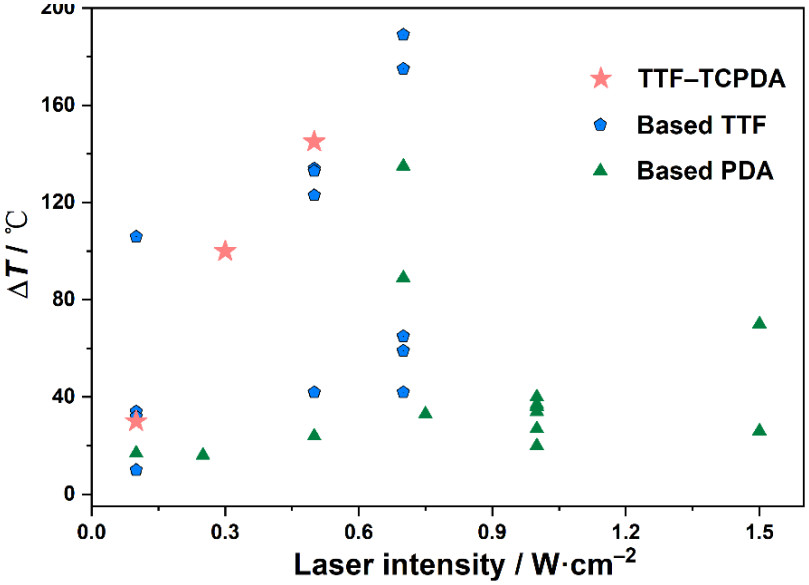

Figure S16. Temperature increase (ΔT) corresponding to the laser intensity of various TTF- and PDA-based photothermal materials illuminated by 660, 808 or 980 nm laser

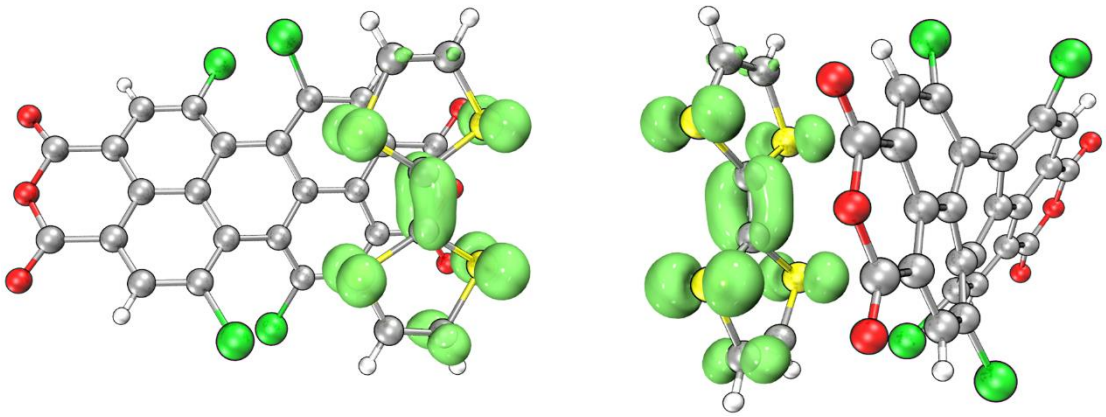

Figure S17. Calculated spin density distribution of TTF–TCPDA at the B3LYP/6-311+G** D3 (BJ) level

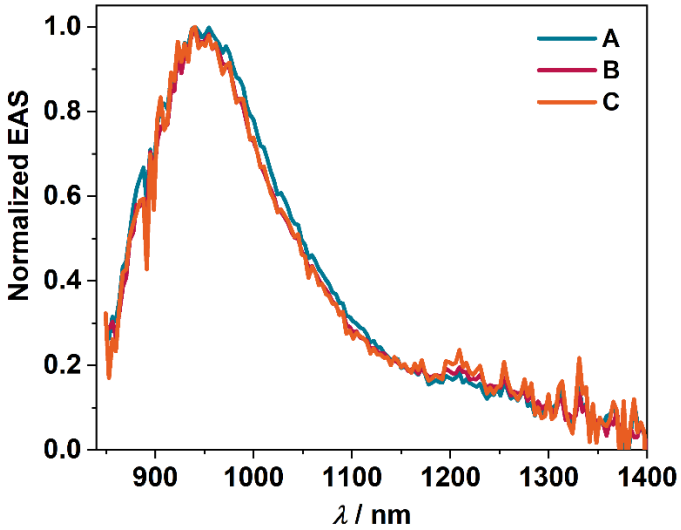

Figure S18. Normalized evolution-associated spectra.

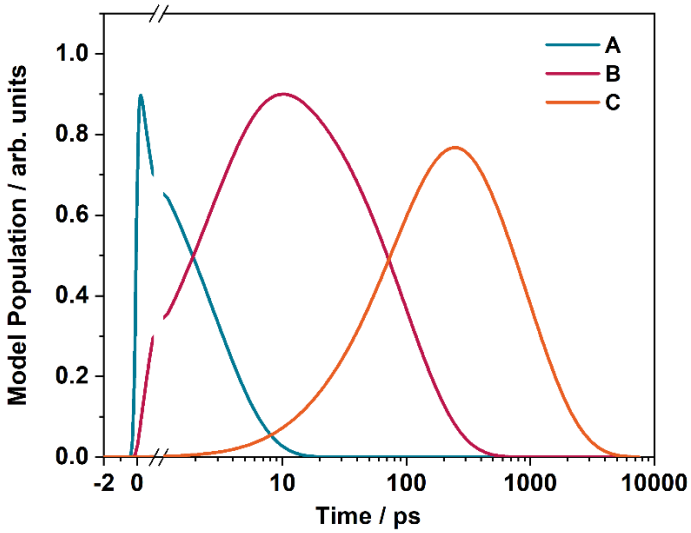

Figure S19. Model populations from kinetic analysis.

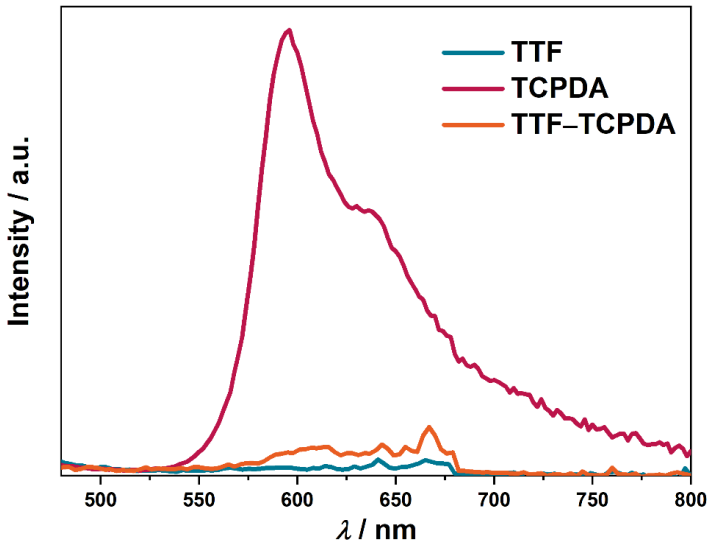

Figure S20. Solid-state fluorescence emission spectra (λ_{ex} = 360 nm) of TTF, TCPDA, and TTF–TCPDA at room temperature.

Photothermal conversion efficiency (η): The accurate photothermal conversion efficiency (η) of these materials was calculated according to a previously described method[9]. In general, each powdery sample was suspended in a 2-mL solution of THF (10 mg/mL) at room temperature (26 °C). The mixture was irradiated (1064 nm, 0.3 W·cm^{-2}) for 10 min. Then the laser was shut off to allow the system to cool down to room temperature naturally. Both the temperature-rising and cooling processes were recorded by an IR thermal camera. In addition, the absorbances of the three times diluted suspensions at 1064 nm were measured as 0.62. Detailed calculation methods are shown as follows:

The η can be defined as the fraction of absorbed light energy that is converted to thermal energy, as shown in the following equation:

$$\eta = \frac{hs(\Delta T_{material} - \Delta T_{solvent})}{I(1-10^{-A})}$$

Supplementary Equation 1

Herein, I is the laser power (0.3 mW, 1 cm^2); A is the absorbance of suspension at the wavelength of 1064 nm; $\Delta T_{material}$ and $\Delta T_{solvent}$ represent the temperature changes of the test sample and blank sample, respectively; h is the heat transfer coefficient, and s is the surface area of the container, which are determined from the following equation:

$$hs = \frac{mc}{\tau_s}$$

Supplementary Equation 2

m is the mass of the solvent (the density of THF is 0.89 g·mL^{-1} so m = 2 × 0.89 = 1.78 g); c is the specific heat capacity of the solvent THF (1.96 J·mol^{-1}·°C^{-1}); and τ_s is a time constant, which can be determined in cooling periods from the following equation:

$$t = -\tau_s \ln(\theta)$$

Supplementary Equation 3

θ is a time-dependent dimensionless parameter known as the driving force temperature, which is defined as follows:

$$\theta = \frac{T - T_{Surr}}{T_{Max} - T_{Surr}}$$

Supplementary Equation 4

T_{Max} (34 °C) and T_{Surr} (26 °C) are the maximum steady-state temperature and the environmental temperature, respectively.

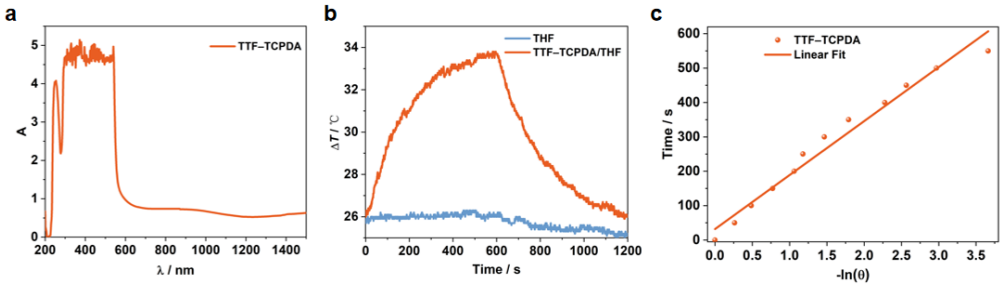

Figure S19. (a) Photothermal conversion curves of THF and TTF–TCPDA in THF and (b) the plot of time versus -ln(θ) from the data recorded during the cooling period.

We are able to get the *hs* = 1.78 × 1.96 / 157 = 0.0222. $\Delta T_{material} - \Delta T_{solvent}$ equals to 8°C. *I* is 0.3 mW where the area of the light spot is 1 cm^2, and *A* is 0.62 . Thus, the 1064-nm η value of TTF–TCPDA is calculated as η = 0.0222 × 8 / 0.3 / (1 – $10^{-0.62}$) = 78 %.

Table S4. Summary of previous results of similar TTF–TCPDA or TTF/TCPDA-based NIR photothermal properties in the literature.

Categories	Samples	Laser λ_{ex} / nm	Laser Intensity / W cm^{-2}	Temperature Range (ΔT / K)	Time	Reference
Organic Material	**TTF–TCPDA**	**1064**	**0.1**	**35**	**20 s**	**This work**
	TTF–TCPDA	**1064**	**0.3**	**100**	**20 s**	**This work**
	TTF–TCPDA	**1064**	**0.5**	**145**	**20 s**	**This work**
	PER-TCNQNPs[10]	1064	1	34	12 min	*Angew. Chem. Int. Ed.* **2021**, *60*, 11758–11762
	2MPT2$^+$–CB[8][11]	1064	0.5	20	5 min	*Angew. Chem. Int. Ed.* **2019**, *58*, 15526–15531
	TTF–F4TCNQ[12]	1064	1	44	10 min	*Adv. Mater*. **2022**, *34*, 2201706
	TMB–F4TCNQ[13]	1060	1	24	10 min	*Angew. Chem. Int. Ed.* **2021**, *60*, 8157–8163
	TMB–TCNQ[13]	1060	1	18	10 min	
	Py–BPy^{2+}COF[14]	1064	1	65	5 min	*J. Am. Chem. Soc.* **2019**, *141*, 14433−14442
	H-TTC/LAG[15]	1064	1	140	15 s	
	H-TTC/LAG[15]	1064	0.5	47	15 s	*CCS Chem.* **2022**, *4*, 2333–2343
	H-TTC/LAG[15]	1064	0.1	15	15 s	
	BAF4 NPs[16]	1064	0.75	35	15 min	*Angew. Chem. Int. Ed.* **2021**, *60*, 22376–22384
	CPDT–T[17]	1064	0.3	13	12 min	
	CPDT–T[17]	1064	0.5	19	12 min	*Chem. Commun*. **2022**, *58*, 6340–6343
	CPDT–T[17]	1064	0.8	29	12 min	
	Et-F4 NPs[18]	1064	0.2	6	10 min	

	Et-F4 NPs[18]	1064	0.6	17	10 min	*J. Mater. Chem. B* **2021**, *9*, 8300–8307
	Et-F4 NPs[18]	1064	1	28	10 min	
	PDPPTBZ NPs[19]	1064	0.3	18	5 min	*Nanoscale* **2019**, *11*, 7754–7760
	TBDOPV–DT NPs[20]	1064	0.9	26	10 min	*ACS Appl. Mater. Interfaces* **2018**, *10*, 7919−7926
	P1 NPs[21]	1064	1	40	5 min	*Adv. Mater*. **2018**, *30*, 1802591
	Nano-BFF[22]	1064	0.5	9	5 min	
	Nano-BFF[22]	1064	1	27	5 min	*Nat Commun*. **2021**,*12*, 218.
	Nano-BFF[22]	1064	1.5	35	5 min	
Inorganic Material	Au−Cu_9S_5 NPs[23]	1064	0.5	12	5 min	
	Au−Cu_9S_5 NPs[23]	1064	0.6	18	5 min	*J. Am. Chem. Soc*. **2014**, *136*, 15684−15693
	Au−Cu_9S_5 NPs[23]	1064	0.7	20	5 min	
	Au@$Cu_{2-x}S$[24]	1064	0.7	20	10 min	*Adv. Mater*. **2016**, *28*, 3094–3101
	2D Nb_2C NSs[25]	1064	0.5	7	5 min	
	2D Nb_2C NSs[25]	1064	1	19	5 min	*J. Am. Chem. Soc*. **2017**, *139*, 16235−16247
	2D Nb_2C NSs[25]	1064	1.5	35	5 min	
	H-SiOxNPs[26]	1064	1	23	20 min	*Biomaterials* **2017**, *143*, 120–129
	Pt spirals[27]	1064	0.2	7	15 min	
	Pt spirals[27]	1064	0.6	19	15 min	*Adv. Mater*. **2019**, *31*, 1904836
	Pt spirals[27]	1064	1.2	33	15 min	
	Fe_2P[28]	1064	0.15	15	10 min	
	Fe_2P[28]	1064	0.3	25	10 min	*Angew. Chem. Int. Ed.* **2019**, *131*, 2429–2434
	Fe_2P[28]	1064	0.5	43	10 min	

	Fe_2P[28]	1064	0.75	50	10 min	
TTF-based	Tri-PMDI-TTF[29]	808	0.7	65	200 s	*Chem. Commun.* **2020**, *56*, 5223–5226
	DTC co-crystal[30]	808	0.7	42	10 min	*Angew. Chem. Int. Ed.* **2018**, *130*, 4027–4031
	Co-MOF film[31]	808	0.5	134	25 s	*Chem. Eur. J.* **2021**, *27*, 11050–11055
	Zn-MOF[32]	808	0.1	106	24 s	*Inorg. Chem*. **2022**, *61*, 3078–3085
	Dy–2D-MOF[33]	808	0.1	34	240 s	*Angew. Chem. Int. Ed.* **2021**, *60*, 4789–4795
	Dy–m-TTFTB[34]	808	0.1	10	15 s	
	Dy–m-TTFTB	808	0.5	42	15 s	*Chem. Sci.* **2022**, *13*, 1657–1664
	Dy–m-TTFTB	808	0.7	59	15 s	
	I_3−@DymTTFT[34]	808	0.1	32	15 s	
	I_3 −@Dy-mTTFT	808	0.5	123	15 s	*Chem. Sci.* **2022**, *13*, 1657–1664
	I_3 −@Dy-mTTFT	808	0.7	175	15 s	
	AgNPs@Dy-mTTFTB[34]	808	0.1	32	15 s	
	AgNPs@Dy-mTTFTB	808	0.5	133	15 s	*Chem. Sci.* **2022**, *13*, 1657–1664
	AgNPs@Dy-mTTFTB	808	0.7	189	15 s	
PDA-based	Zr-PDI•–powder[35]	808	0.7	135	10 s	*Nat. Commun*. **2019**, *10*, 767.
	Zr-PDI•– film[35]	808	0.7	89	100 s	*Nat. Commun*. **2019**, *10*, 767.
	BPDI/(CB[7])2[36]	808	1	20	10 min	*Chem. Sci*. **2015**, *6*, 3975–3980
	CPPDI [37]	808	1	40	30 min	*Angew. Chem. Int. Ed.* **2017**, *56*, 16239–16242
	PPDI-NPs[38]	660	0.25	16	10 min	
	PPDI-NPs[38]	660	0.75	33	10 min	*Theranostics* **2020**, *10*, 1

	PBI-[GY]2[39]	808	1	27	15 min	
	PBI-[GD]2[39]	808	1	34	15 min	*Chem. Commun.* **2018**, *54*, 2208–2211
	QDI-NPs[40]	808	0.1	17	10 min	
	QDI-NPs[40]	808	0.5	24	10 min	*Angew. Chem. Int. Ed.* **2019**, *58*, 1638–1642
	QDI-NPs[40]	808	1	37	10 min	
	TNMs[41]	660	1	36	10 min	*ACS Nano* **2017**, *11*, 3797–3805
	PDIHOF(PFC55)[42]	980	1.5	26	20 s	
	UCNPs@PFC55[42]	980	1.5	70	20 s	*Angew. Chem. Int. Ed.* **2021**, *60*, 1–8

7. References

1 A. Ellern, J. Bernstein, J. Y. Becker, S. Zamir, L. Shahal and S. Cohen, *Chem. Mater.,* 1994, **6**, 1378-1385.

2 P. J. Stephens, F. J. Devlin, C. F. Chabalowski and M. J. Frisch, *J. Phys. Chem.,* 1994, **98**, 11623-11627.

3 S. Grimme, J. Antony, S. Ehrlich and H. Krieg, *J. Chem. Phys.,* 2010, **132**, 154104.

4 S. Simon, M. Duran and J. J. Dannenberg, *J. Chem. Phys.,* 1996, **105**, 11024-11031.

5 M. Frisch, G. W. Trucks, H. B. Schlegel, G. E. Scuseria, M. A. Robb, J. R. Cheeseman, G. Scalmani, V. Barone, B. Mennucci and G. Petersson, Gaussian, Inc., Wallingford CT, 2009.

6 T. Lu and F. Chen, *J. Comput. Chem.,* 2012, **33**, 580-592.

7 W. Humphrey, A. Dalke and K. Schulten, *J. Mol. Graph., **1996**, 14*, 33-38.

8 R. L. Martin, *J. Chem. Phys.,* 2003, **118**, 4775-4777.

9 B.-T. Liu, X.-H. Pan, D.-Y. Zhang, R. Wang, J.-Y. Chen, H.-R. Fang and T.-F. Liu, *Angew. Chem. Int. Ed.,* 2021, **60**, 25701-25707.

10 S. Tian, H. Bai, S. Li, Y. Xiao, X. Cui, X. Li, J. Tan, Z. Huang, D. Shen, W. Liu, P. Wang, B. Z. Tang and C. S. Lee, *Angew. Chem. Int. Ed.,* 2021, **60**, 11758-11762.

11 B. Tang, W.-L. Li, Y. Chang, B. Yuan, Y. Wu, M.-T. Zhang, J.-F. Xu, J. Li and X. Zhang, *Angew. Chem. Int. Ed.,* 2019, **58**, 15526-15531.

12 Y. Chen, P. He, D. Jana, D. Wang, M. Wang, P. Yu, W. Zhu and Y. Zhao, *Adv. Mater.,* 2022, **34**, e2201706.

13 C. Ou, W. Na, W. Ge, H. Huang, F. Gao, L. Zhong, Y. Zhao and X. Dong, *Angew. Chem. Int. Ed.,* 2021, **60**, 8157-8163.

14 Z. Mi, P. Yang, R. Wang, J. Unruangsri, W. Yang, C. Wang and J. Guo, *J. Am. Chem. Soc.,* 2019, **141**, 14433-14442.

15 J. Xu, Z. Yin, L. Zhang, Q. Dong, X. Cai, S. Li, Q. Chen, P. Keoingthong, Z. Li, L. Chen, Z. Chen and W. Tan, *CCS Chem.,* 2022, **4**, 2333-2343.

16 Z. Jiang, C. Zhang, X. Wang, M. Yan, Z. Ling, Y. Chen and Z. Liu, *Angew. Chem. Int. Ed.,* 2021, **60**, 22376-22384.
17 W. Jia, F. Huang, Q. Zhang, L. Zhao, C. Li and Y. Lu, *Chem. Commun.,* 2022, **58**, 6340-6343.
18 W. Ge, Y. Xu, C. Liu, W. Xu, Y. Zhang, W. Si, W. Zhao, C. Ou and X. Dong, *J. Mater. Chem. B,* 2021, **9**, 8300-8307.
19 Y. Yang, J. Chen, Y. Yang, Z. Xie, L. Song, P. Zhang, C. Liu and J. Liu, *Nanoscale,* 2019, **11**, 7754-7760.
20 T. Sun, J.-H. Dou, S. Liu, X. Wang, X. Zheng, Y. Wang, J. Pei and Z. Xie, *ACS Appl. Mater. Interfaces,* 2018, **10**, 7919-7926.
21 B. Guo, Z. Sheng, D. Hu, C. Liu, H. Zheng and B. Liu, *Adv. Mater.,* 2018, **30**, e1802591.
22 H. Xiang, L. Zhao, L. Yu, H. Chen, C. Wei, Y. Chen and Y. Zhao, *Nat. Commun.,* 2021, **12**, 218.
23 X. Ding, C. H. Liow, M. Zhang, R. Huang, C. Li, H. Shen, M. Liu, Y. Zou, N. Gao, Z. Zhang, Y. Li, Q. Wang, S. Li and J. Jiang, *J. Am. Chem. Soc.,* 2014, **136**, 15684-15693.
24 M. Ji, M. Xu, W. Zhang, Z. Yang, L. Huang, J. Liu, Y. Zhang, L. Gu, Y. Yu, W. Hao, P. An, L. Zheng, H. Zhu and J. Zhang, *Adv. Mater.,* 2016, **28**, 3094-3101.
25 H. Lin, S. Gao, C. Dai, Y. Chen and J. Shi, *J. Am. Chem. Soc.,* 2017, **139**, 16235-16247.
26 X. Yu, K. Yang, X. Chen and W. Li, *Biomaterials,* 2017, **143**, 120-129.
27 Q. Wang, H. Wang, Y. Yang, L. Jin, Y. Liu, Y. Wang, X. Yan, J. Xu, R. Gao, P. Lei, J. Zhu, Y. Wang, S. Song and H. Zhang, *Adv. Mater.,* 2019, **31**, e1904836.
28 Y. Liu, W. Zhen, Y. Wang, J. Liu, L. Jin, T. Zhang, S. Zhang, Y. Zhao, S. Song, C. Li, J. Zhu, Y. Yang and H. Zhang, *Angew. Chem. Int. Ed.,* 2019, **58**, 2407-2412.
29 D. Wang, X. Kan, C. Wu, Y. Gong, G. Guo, T. Liang, L. Wang, Z. Li and Y. Zhao, *Chem. Commun.,* 2020, **56**, 5223-5226.
30 Y. Wang, W. Zhu, W. Du, X. Liu, X. Zhang, H. Dong and W. Hu, *Angew. Chem. Int. Ed.,* 2018, **57**, 3963-3967.
31 T. Yan, Y.-Y. Li, J. Su, H.-Y. Wang and J.-L. Zuo, *Chem. Eur. J.*, 2021, **27**, 11050-11055.
32 T. Yan, Y.-Y. Li, Q.-Y. Gu, J. Li, J. Su, H.-Y. Wang and J.-L. Zuo, *Inorg. Chem.,* 2022, **61**, 3078-3085.
33 J. Su, N. Xu, R. Murase, Z.-M. Yang, D. M. D'Alessandro, J.-L. Zuo and J. Zhu, *Angew. Chem. Int. Ed.,* 2021, **60**, 4789-4795.
34 J. Su, P. Cai, T. Yan, Z.-M. Yang, S. Yuan, J.-L. Zuo, H.-C. Zhou, *Chem. Sci.,* 2022, **13**, 1657-1664.
35 B. Lu, Y. Chen, P. Li, B. Wang, K. Mullen, M. Yin, *Nat. Commun.,* 2019, **10**, 767.
36 Y. Jiao, K. Liu, G. Wang, Y. Wang, X. Zhang, *Chem. Sci.,* 2015, **6**, 3975-3980.
37 Y. Yang, P. He, Y. Wang, H. Bai, S. Wang, J.-F. Xu and X. Zhang, *Angew. Chem. Int. Ed.,* 2017, **56**, 16239-16242.
38 J. Li, C. Liu, Y. Hu, C. Ji, S. Li and M. Yin, *Theranostics,* 2020, **10**, 166-178.
39 L. Cui, Y. Jiao, A. Wang, L. Zhao, Q. Dong, X. Yan and S. Bai, *Chem. Commun.,* 2018, **54**, 2208-2211.
40 C. Liu, S. Zhang, J. Li, J. Wei, K. Müllen and M. Yin, *Angew. Chem. Int. Ed.,* 2019, **58**, 1638-1642.
41 S. Zhang, W. Guo, J. Wei, C. Li, X.-J. Liang and M. Yin, *ACS Nano,* 2017, **11**, 3797-3805.
42 B.-T. Liu, X.-H. Pan, D.-Y. Zhang, R. Wang, J.-Y. Chen, H.-R. Fang and T.-F. Liu, *Angew. Chem. Int. Ed.,* 2021, **60**, 25701-25707